

Indicial response function for finite-thickness airfoils, a semi-empirical approach

Mac Gaunaa*, Leonardo Bergami† and Joachim Heinz†

Risø National Laboratory for Sustainable Energies,

Technical University of Denmark,

Roskilde, 4000 Denmark

Many wind turbines aeroelastic codes recourse to indicial lift response formulations to evaluate unsteady aerodynamics in attached flow. The indicial response of a finite-thickness airfoil differs from the flat plate one, which is usually adopted through Jones's approximation. The lift response of airfoils with different geometries is determined with a panel code, and approximated by two term exponential functions. An empirical relation is then outlined in order to estimate the indicial response from the profile geometry. Unsteady lift computations are compared to CFD simulations for a harmonic pitching airfoil; the agreement with CFD results is improved by using the estimated indicial response instead of Jones's flat plate expression. Finally, the effects on fatigue and ultimate loads are assessed by using the different indicial lift response function approximations in aeroelastic simulations.

I. Introduction

Aeroelastic simulation tools require aerodynamic models accounting for unsteady aerodynamic effects. The aerodynamic model should be simple, to limit the computations required in a time marching simulation, and, at the same time, complex enough to predict with sufficient accuracy the aerodynamic loads arising on the blade, both in attached and separated (stalled) flow conditions.

A large contribution to the total aerodynamic loading is generated on the outer sections of the blades, which, in modern wind turbines, operate most of the time in attached flow conditions. Unsteady aerodynamic forces in attached flow are frequently described by Beddoes-Leishman^{1,2} types of model, simplified for wind turbine applications by the incompressible fluid assumption. Wind turbine simulation tools based on this approach include, among others, the aeroelastic code HAWC2,^{3,4} Bladed,⁵ and FAST.^{6,7}

In these Beddoes-Leishman derived models, the attached unsteady lift is described, following Theodorsen's theory,⁸ as the sum of two contribution: a non-circulatory and a circulatory one. The non-circulatory lift, or added mass term, can be thought of as originating from the air mass accelerated by the airfoil, and thus only depends on the instantaneous motion of the airfoil. The circulatory lift, on the contrary, carries a memory effect, which originates from the vorticity shed into the wake to compensate the change of circulation around the airfoil.

The circulatory lift for an airfoil undergoing arbitrary motion is obtained from a Duhamel's superposition integral of indicial step responses:⁹

$$L_c = 2\pi\rho Ub \left[w_{3/4}(0) \cdot \Phi(\tau) + \int_0^\tau \frac{dw_{3/4}}{d\sigma} \Phi(\tau - \sigma) d\sigma \right]. \quad (1)$$

Where, b is the half-chord length, $w_{3/4}$ is the downwash at the three-quarters chord, and the dimensionless variable τ is the distance traveled by the airfoil, measured in half-chords:

$$\tau = \frac{Ut}{b}. \quad (2)$$

The indicial response function $\Phi(\tau)$ represents the ratio between the actual unsteady lift and the corresponding steady value, following a unit step change in the angle of attack. Wagner⁹ applies analytical

*Senior Scientist, Wind Energy, AIAA Senior Member.

†Ph.D. Student, Wind Energy, AIAA Student Member.

methods to define the indicial response function for a flat plate in incompressible flow; the resulting function tends asymptotically to unit and starts from a value of 0.5 at $\tau = 0$, indicating that half the change in circulatory lift is obtained at the initial instant. Wagner’s function is not formulated in simple analytical terms, rendering Duhamel integration rather complex; to obviate the problem, the response function is approximated as a linear combination of exponential terms:⁹

$$\Phi \approx 1 - \sum A_i \exp^{b_i \tau}; \quad (3)$$

Jones¹⁰ proposes a two term approximation for the flat plate indicial response (fig. 3),

$$\Phi = 1 - 0.165 \exp^{-0.045\tau} - 0.335 \exp^{-0.3\tau} . \quad (4)$$

Several references report indicial lift responses for airfoils with finite thickness that differ from the flat plate response. Giesing¹¹ shows indicial curves below the flat plate one for the response of Von Mises and Jukowsky airfoils; similar results are obtained by Basu and Hancock,¹² who simulate the step response of a Von Mises airfoil with a panel code. Chow¹³ concludes that finite thickness airfoils have a slower step response, and the response speed decreases as the airfoil thickness and trailing edge angle are augmented.

More recently, Gaunaa¹⁴ applies a panel code method to compute the response of NACA symmetric airfoils with different thicknesses, and shows that the response curve tends to the flat plate one as the thickness is reduced. In Hansen *et al.*,⁴ the same panel code method is used to simulate the step response of a 24% thick Risø A1 airfoil; the resulting indicial response is approximated by a two term exponential function which is then supplied to the Beddoes-Leishman model described in the report. Hansen *et al.* present lift versus angle of attack simulations loops for an airfoil undergoing harmonic pitch variations; they show that the loop obtained with Jones’s indicial approximation significantly differs from the one obtained with the Risø airfoil response function, and the latter is closer to the results obtained with dynamic Navier-Stokes computations. Buhl *et al.*¹⁵ follow a similar approach to approximate the step response of a Risø B1-18 airfoil, and in Bergami¹⁶ is shown that a stability analysis based on the indicial function for the B1-18 response returns flutter limits that differ from the ones based on Jones’s flat plate indicial approximation.

Nevertheless, Jones’s approximation for the flat plate response remains a widespread standard in incompressible attached flow models; no investigations have been so far encountered proposing alternative approximations for finite thickness airfoil, or evaluating the effects that different indicial response approximations would have on wind turbine load simulations.

The present work seeks an empirical relation between the airfoil indicial lift response, and its geometric characteristics. Gaunaa’s¹⁴ panel code is used to compute the indicial response for a set of airfoils with different geometries; the indicial response curves are approximated with Jones-like two term exponential functions, in the form of eq. (3). The different airfoils and corresponding indicial responses provides the dataset on which regression methods are applied to outline the empirical function.

The empirical relation is tested on airfoils not belonging to the previous dataset, and unsteady lift forces for airfoils in harmonic pitching motion are computed from the resulting indicial response function. The lift force is compared to CFD simulations and to the forces obtained when using the classic Jones’s flat plate approximation.

The effects of the response function approximations on wind turbine loads predictions are then assessed by running aeroelastic simulations of the NREL 5-MW reference turbine, and applying different approximations to the aerodynamic model.

II. Model and method

In order to estimate the effects that different airfoil geometries might have on the indicial response functions, several airfoil profile shapes have been considered. Each airfoil profile is discretized into panels, and the circulatory lift indicial response is simulated using a panel code. The simulated response is fitted with a two term exponential function, and an empirical function is sought in order to link the coefficients defining the exponential indicial function (A_1, A_2, b_1, b_2 , eq. (3)) to the airfoil geometric characteristics.

II.A. Airfoil profiles

A preliminary investigation considered airfoil shapes taken from the modified NACA 4-digits family.¹⁷ The profiles are obtained as a superposition of thickness distribution to airfoil mean line; both the thickness distribution and the mean line camber are described by simple polynomial functions. The

mean line function is defined by two parameters,^a and the thickness function by three:^b a set of five parameters completely characterizes every airfoil in the family.

For this family of airfoils, the linear term dominates the thickness distribution close to the trailing edge. The result is a trailing edge angle wider than for airfoils with the same thickness from other families (fig. 1); as well as that, throughout the NACA 4-digits family, the ratio of airfoil thickness over trailing edge angle is almost constant.

To overcome such limitation in the airfoil shapes, the thickness distribution is scaled with an half-cosine function aft the point of maximum thickness x_{thm} . The scaling function introduces an additional parameter k_{cos} :

$$\frac{t_{mod}}{t_{NACA}} = \begin{cases} 1 & \text{for } x \leq x_{thm} \\ 0.5 + 0.5 \cos\left(\pi \frac{x-x_{thm}}{1-x_{thm}} k_{cos}\right) & \text{for } x > x_{thm} \end{cases} \quad (5)$$

The thickness modification allows for profiles with sharper trailing edges (fig. 1), and introduces further variety in the dataset of investigated airfoil shapes.

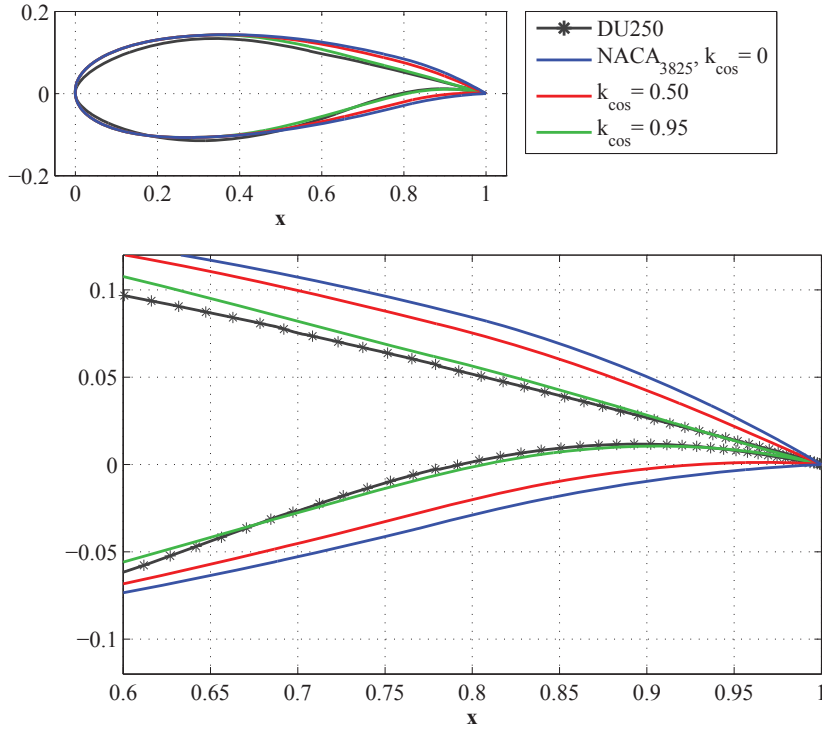


Figure 1. Airfoil shapes and Trailing Edge angle. The NACA-3825 airfoil (blue line) has the same thickness and maximum camber as the DU91-W2-250 (black line), but a wider TE angle. The cosine thickness modification (red and green lines) yields to a sharper trailing edge.

II.B. Panel code simulation

The indicial response of the airfoil is obtained from panel code simulations. The code has been developed by Gaunaa,¹⁴ following a Hess's formulation,¹⁸ where the singularity elements are given by: constant strength source distribution, constant strength vortex distributions, and two dimensional point vortices in the wake. A detailed description of the model, and its validation are presented in Gaunaa.¹⁴

Applying small time steps, the panel code simulation returns an unusual behavior of the indicial lift, which starts decreasing from a value above the steady one. Such results are similar to the transient behavior described by Graham¹⁹ for an airfoil in impulsively started flow, where the roll up of wake vorticity dominates the unsteady aerodynamics. In these conditions, the indicial lift presents an initial

^aMean line parameters: abscissa and chord-wise ordinate of the point of the mean line giving the maximum camber. They correspond to first and second digit in the NACA numbering.

^bThickness distribution parameters: maximum thickness in chord percentage (3rd and 4th digits in NACA numbering), chord-wise ordinate of the point with maximum thickness, radius of curvature for the leading edge.

singularity: it first decreases with time, and only subsequently monotonically increases, as in Wagner’s indicial response function.

As observed by Graham, an airfoil does not encounter a truly impulsive start in realistic conditions. The wake dynamic is thus generally dominated by downstream convection of the vorticity, rather than roll up, and the indicial lift increases monotonically to the steady value.

The present investigation focuses on the response of airfoils in realistic conditions, therefore, time steps are selected as large as sufficient to avoid the impulsive start singularity. The response at time zero is then obtained from a quadratic extrapolation of the first computed points.

II.C. Exponential curve fitting

The simulated indicial response can be approximated by a n -terms exponential function, eq. (3); the more terms, the better the approximation. It is chosen to use a two terms function, which returns a sufficiently accurate approximation (fig.3) and keeps similarity with Jones’s expression:

$$\Phi = 1 - A_1 \exp^{b_1 \cdot \tau} - A_2 \exp^{b_2 \cdot \tau} . \quad (6)$$

The two term function is defined by 4 coefficients: b_1 giving the decay of the fast term, b_2 for the slow decaying term, and A_1 and A_2 giving the weights of the two components. The coefficients are found through minimization of the weighted sum of the squared differences between the simulated response and the fitted curve.

The weight function is set to be equal to the difference between the simulated indicial response, and the unit steady value. In this way, the minimization algorithm values more the fitting for points in the initial part of the transient, reducing the influence from the almost stationary tail of the indicial curve; for the same purpose, the curve tail is truncated where the response reaches 99.9% of the final value.

II.D. Profile Surface Angle

A preliminary investigation indicates that the lift response coefficients are related to the angle between upper and lower surface of the profile, especially close to the trailing edge, as it was also observed in Chow.¹³

It is therefore chosen to represent the geometric characteristics of an airfoil in terms of a *profile surface angle* $\beta(x)$. For a given chord-wise coordinate \tilde{x} , $\beta(\tilde{x})$ is defined as the angle between two lines that originate at the trailing edge and intersect the profile upper and lower surface at the points of chord-wise coordinate \tilde{x} , figure 2.

Each airfoil is thus characterized by a set of angles $\beta(x)$, measured on the profile geometry at given locations x ; the same airfoil is also associated to a set of lift response coefficients (A_1, A_2, b_1, b_2) . An analytical relation between the lift coefficients and the angles β would thus allow to estimate the indicial lift response of an airfoil from simple measurement of its geometric characteristics.

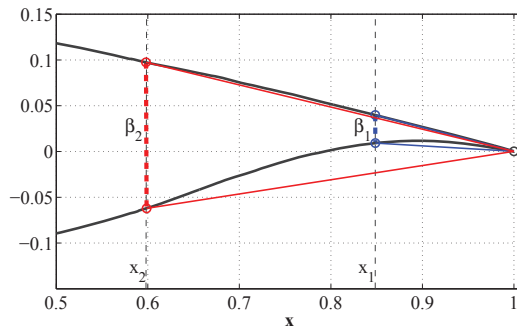


Figure 2. Profile angle β at chord-wise position x_1 and x_2

III. Results

III.A. Preliminary investigation

A preliminary investigation is carried out on airfoils shapes from the NACA 4-digits family. It is observed that the indicial lift response is scarcely influenced from variations of mean line camber and leading edge radius; on the contrary, the airfoil thickness and the location of its maximum along the chord strongly affect the indicial response function.

As also observed in Gaunaa¹⁴ and Chow,¹³ thicker airfoils have a slower response and the the indicial lift functions have a starting value below the $\Phi_{(\tau=0)} = 0.5$ of the flat plate; as the airfoil thickness is reduced, the response tends to the flat plate one, figure 3.

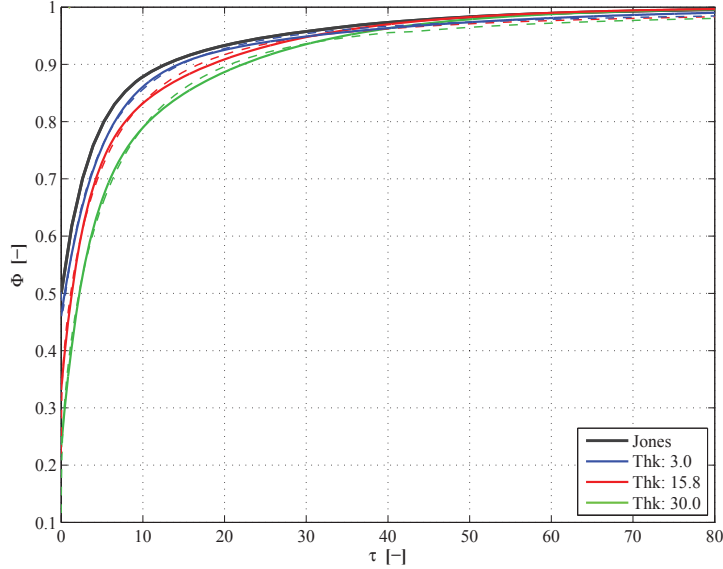


Figure 3. Indicial lift response function for NACA 44xx airfoils with different thicknesses and for a flat plate (Jones's coefficients). Dashed lines: response simulated by the panel code; full lines: two terms exponential approximation.

The profile angle measured at the trailing edge $\beta(x_{TE})$ is used to characterize the geometry of the airfoils in the family. The parameter $\beta(x_{TE})$, in fact, is sufficient to account for most of the variations observed in the lift response coefficients of this family of airfoil.

This simple relation does not hold for airfoils outside the 4-digits family, hence the need to extend the pool of investigated profile shapes by introducing the cosines modification on the thickness distribution, eq.(5).

III.B. Enlarged dataset of airfoils

Several combinations of airfoil thickness and cosine scaling parameter are used to generate a dataset of airfoil profiles; for each profile, the panel code simulates the indicial lift response, which is then fitted with the two term approximation. Each airfoil profile i in the dataset, is thus associated with a set of four lift response coefficients ($A_1^i, A_2^i, b_1^i, b_2^i$, as in eq. (6)), and a set of profile angles measured at different chord-wise locations: $\beta(x)_i$. A relation is sought between the lift coefficients and the profile angle at few selected locations.

At first, it is assumed that the lift coefficients (dependent variable or regressand) can be expressed as a quadratic function of the profile angle at one location $\beta(\tilde{x})$ (independent variable or regressor):

$$y_i = a_0 + a_1\beta(\tilde{x}) + a_2\beta(\tilde{x})^2, \quad \forall \text{ profile } i. \quad (7)$$

Where the regressand y_i is one of the lift coefficients for the profile (A_1^i, A_2^i, b_1^i , or b_2^i); a_0, a_1, a_2 are the regression parameters, which are constants for all the airfoil profiles i in the dataset, $i = 1 \dots N_{prof}$; each of the four lift coefficients gives a different set of regression parameters.

The set of regression parameters that better explains the variation in the dataset corresponds to the parameters for the parabolic curve that better fits the points with coordinates $(\beta(\tilde{x}); y)_i$. The problem is formulated as a linear model regression, and is solved with an ordinary least square regressor, for different locations \tilde{x} of the profile angle measurement.

The coefficient of determination $r^2(x)$ evaluates the ‘quality’ of the regression; the minimum points of the curves $(1 - r^2)$ (fig. 4, top) indicate the optimal locations x^* : the corresponding profile angles $\beta(x^*)$ give the regression with the best explanation of the variation observed in the lift coefficients.

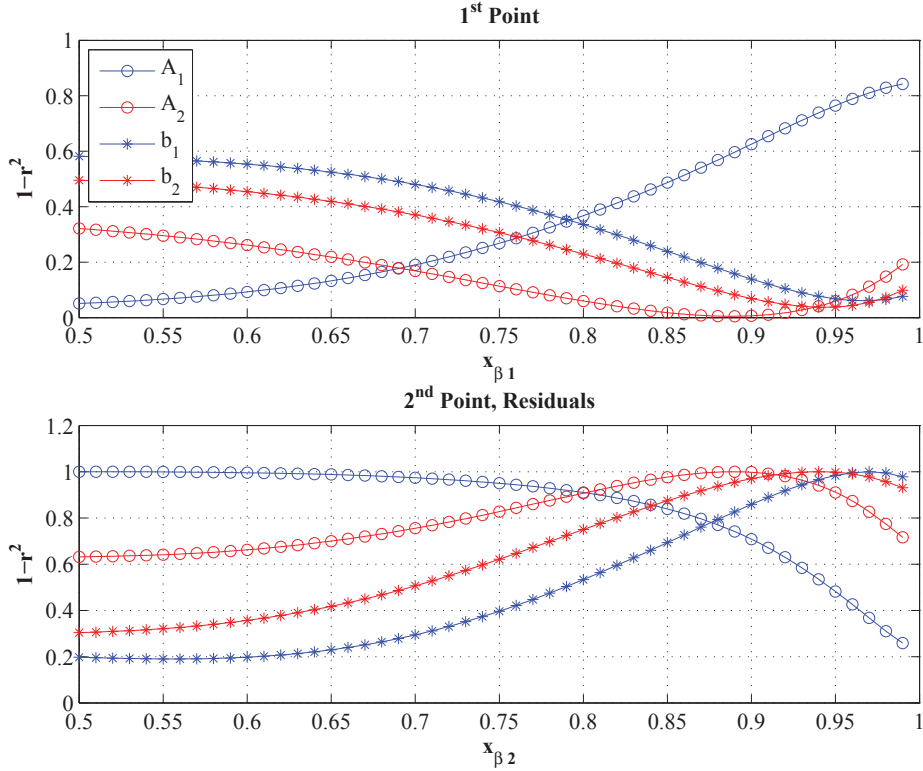


Figure 4. One minus coefficient of determination versus the location of the profile angle measurement point; the curve minima correspond to the best regression. Top: location of the first profile-angle point x_1 , regression on the dataset. Bottom: location of the second profile-angle point x_2 , regression on the residuals.

Although optimally placed, measurements of the profile angle at only one point are not sufficient to account for all the variation in the lift coefficients. A profile angle measured in a second point x_2 is introduced in the empirical function: $y_i = f(\beta_{x_1}, \beta_{x_2})$. The optimal location of the second point is determined from the coefficient of determination r^2 in a second regression, where the regressand variables $y_{i,2}$ are the residuals from the first regression: $y_{i,2} = y_i - \hat{y}_i$. The minima of the $(1 - r^2)$ curves (figure 4, bottom) give the optimal placement for the second profile angle measurement β_{x_2} . Note that, since the second regression (fig. 4, bottom) fits the residuals of the first, whenever the second measurement point x_2 coincides with the first x_1 , the coefficient $(1 - r^2)$ is one, which indicates that the second point, being identical to the first, does not contribute to the data explanation.

The regression analysis indicate for each lift coefficient the optimal locations of the two measurements points for the profile angle. The optimal locations are slightly modified to reduce the total number of points to 3, and the resulting pair of points are reported in the first columns of table 1. For each lift response coefficient, one point is located close to the airfoil trailing edge, the other to mid-chord; it is thus confirmed that the geometric parameters that more affects the indicial lift response are the airfoil thickness (roughly proportional to the profile angle at mid-chord), and the profile ‘opening’ near the trailing edge.

Each indicial lift coefficient is expressed as a quadratic function of the profile angle β at two given locations (x_1 and x_2) along the profile:

$$y_i = a_0 + a_{11}\beta_{x_1} + a_{12}\beta_{x_1}^2 + a_{21}\beta_{x_2} + a_{22}\beta_{x_2}^2. \quad (8)$$

The profile angle location pair (x_1 and x_2) depends on which of the four lift coefficient is being considered: $y_i = A_1, A_2, b_1$, or b_2 . The regression parameters are found by solving the corresponding ordinary least square problem (table 1). The parameters for the quadratic terms (a_{12}, a_{22}) are rather close to zero, highlighting a dominant linear behavior; nevertheless, no regression parameter admits the zero value inside its 95% confidence interval, thus also the quadratic terms are ‘significant’ in the fitting.

Table 1 reports the profile angle location and the regression parameters for each lift response coeffi-

cient. The regression parameters yield to a set of four empirical equations, one for each lift coefficient, eq. (8); the empirical equations allow then to estimate the lift response function of an arbitrary profile by simply measuring its profile angle in three different locations.

Lift Coef.	x_1	x_2	a_0	a_{11}	a_{12}	a_{21}	a_{22}
A_1	0.95	0.5	3.93E-01	-1.32E-03	3.41E-05	2.06E-05	5.33E-05
A_2	0.88	0.5	1.01E-01	9.41E-03	-7.80E-05	2.35E-03	-9.24E-05
b_1	0.95	0.5	-1.90E-01	-8.35E-03	1.04E-04	-7.16E-03	2.65E-04
b_2	0.95	0.5	-2.83E-02	-1.29E-03	1.85E-05	-1.04E-03	3.44E-05

Table 1. Empirical estimation of the indicial lift response coefficients. Location of the two profile angle measurement points: x_1, x_2 . Regression parameters to be applied in equation (8) for coefficient estimation.

IV. Validation

The set of empirical equations derived in the previous section is tested for three airfoil profiles used on the reference rotor of the MEXICO project:²⁰ DU 91-W2-250, RISOE A1-21, and NACA 64-418. The airfoils have profile shapes commonly employed on wind turbine blades, they differ in thickness and camber characteristics, and none of them was part of the dataset used in the regression.

For each airfoil, the lift coefficients estimated by the empirical relation (circles, in fig. 5) are compared with the ones fitting the indicial response simulated by the panel code (stars). The estimated values are found very close to the panel codes ones, and they give a far better approximation of the indicial lift response than Jones’s coefficients do.

The same plot (fig.5) also reports estimated and panel code coefficients (green circles and stars) for three ‘symmetric profiles’. The symmetric profiles have the same thickness distribution as the previous three airfoils, but a null mean line; in other words, the camber line was ‘subtracted’ from the original airfoils. The change in the mean line has a rather small effect on the lift coefficients, as was also observed in the NACA 4-digits family.

The empirical equations are further tested to verify that plausible lift response functions are obtained for profile angles ranges:

$$\forall \text{ profile } \begin{cases} 2^\circ \leq \beta_{x1} \leq 50^\circ \\ 3^\circ \leq \beta_{x2} \leq 40^\circ \end{cases} . \quad (9)$$

The empirical equation might result in an unreasonable indicial lift response when applied to airfoils outside this range, which corresponds, roughly, to airfoils with a thickness ratio below 40%.

IV.A. CFD comparison

The three profiles are used to simulate unsteady lift forces in harmonic pitching motion. The profiles are hinged at the quarter chord point, the angle of attack is changed from 1° to 3° , with two reduced frequencies: $K = \omega b/U = 0.1$, and a faster one $K = 0.5$.

Lift forces are computed with the analytical model described in Hansen *et al.*;⁴ the model, here simplified for attached flow conditions, is based on superposition of indicial response functions approximated by exponential terms. For each airfoil, three sets of indicial response coefficients are considered: the ones from Jones’s flat plate expression, the estimations from the empirical equation, eq.8, and the ones obtained by exponential fitting of the panel code response.

The resulting lift loops (fig. 6) are compared against CFD simulations. The CFD results were obtained using EllipSys, Risø’s in-house CFD code, developed as a cooperation between the Department of Mechanical Engineering at the Technical University of Denmark and the Department of Wind Energy at Risø National Laboratory.²¹⁻²³

The estimated lift response coefficients are very close to the panel code ones, as in figure 5: the corresponding loops (respectively, blue line and red circles in fig. 6) are thus practically overlapping. The loops based on the estimated response coefficients are much closer to the CFD results (black lines) than the loops with flat plate coefficients, indicating thus a better approximation of the airfoil indicial response. The differences among the loops are increased as the reduced frequency is augmented.

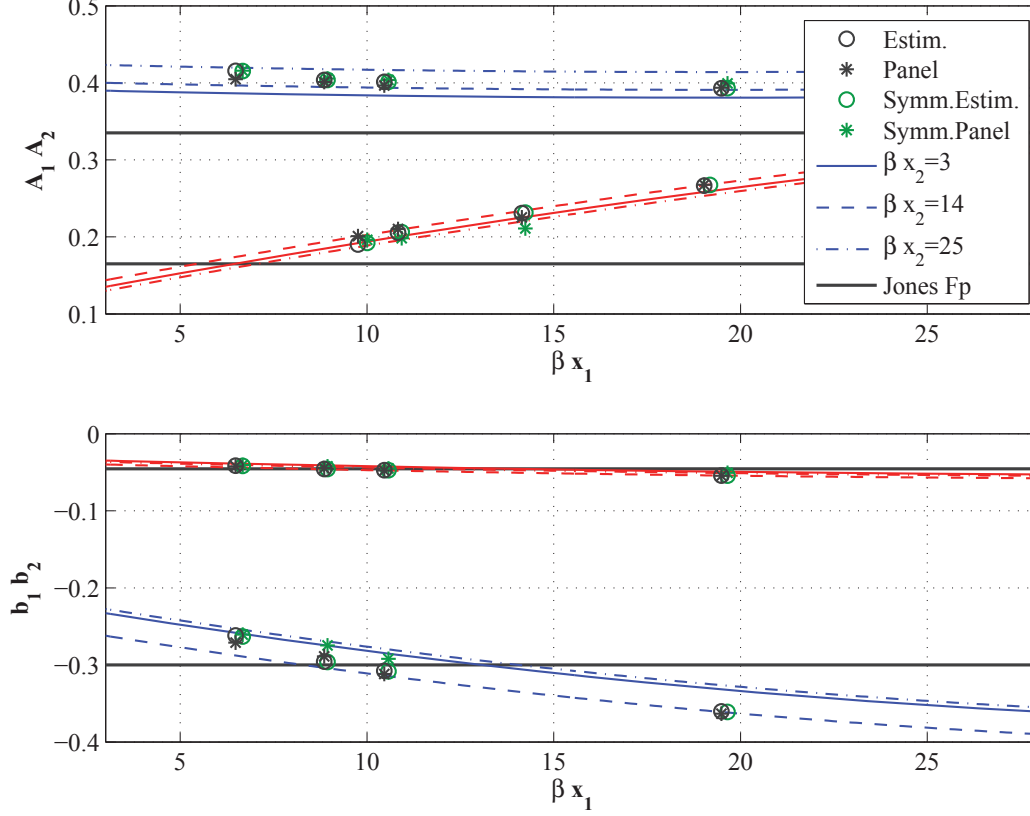


Figure 5. Lift response coefficients as function of the airfoil profile angle at location x_1 . Estimated (circles) and panel code (stars) coefficients for the airfoils: DU 91-W2-250, RISOE A1-21, NACA 64-418 (from the left). The plot reports curves from the empirical estimation function for three arbitrary β_{x_2} profile angles, and the flat plate coefficients from Jones's approximation. The green circles and stars refer to airfoil shapes obtained by changing the mean line of the airfoils to a zero line (symmetric airfoils).

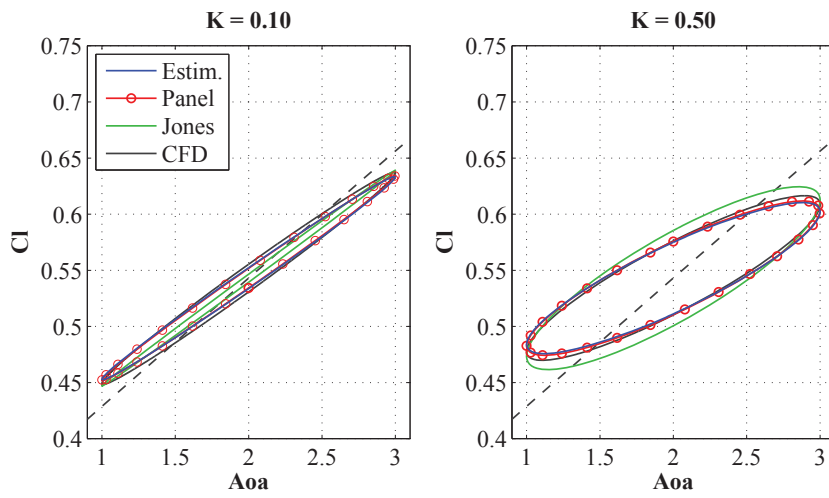
V. Relevance to Load Simulation

In most aeroelastic codes for wind turbine loads simulation, the indicial lift coefficients are given by Jones's approximation of the flat plate response. As observed in the previous sections, the response of an airfoil with finite thickness differs from the flat plate one, and the higher is the reduced frequency of the unsteady motion, the larger the difference in the resulting aerodynamic forces.

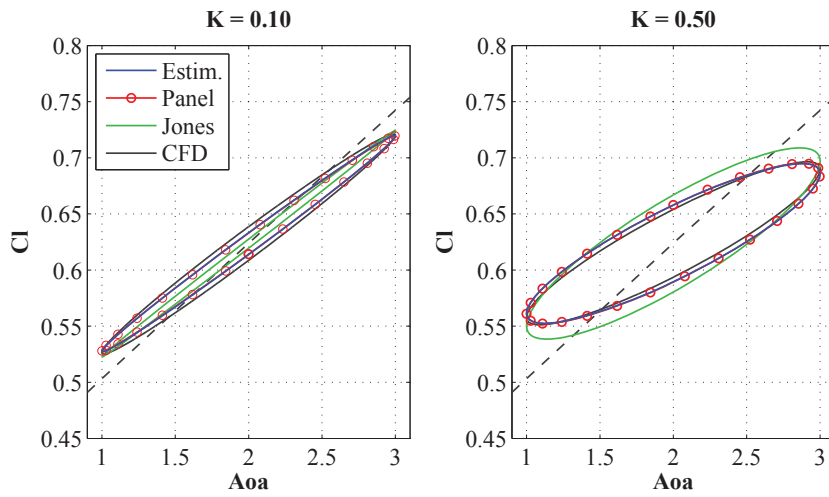
To assess how this difference affects the simulated wind turbine loads, the response of the NREL 5-MW reference wind turbine²⁴ is simulated using the aeroelastic code Hawc2.³ Three different set-ups of the aerodynamic model are considered, where the coefficients for the indicial lift response function are given by:

- Jones's flat plate response. The default value in most of the codes.
- Estimated coefficients for the DU 91-W2-250 airfoil. The airfoil is similar to the one used at the blade mid-span of the NREL 5-MW rotor; the current version of the aeroelastic code does not allow to vary the lift response coefficients along the blade span, therefore the DU 91-W2-250 response approximation is applied to the whole blade.
- Quasi-Steady approximation ($A_1 = A_2 = 0$), also a rather common assumption.

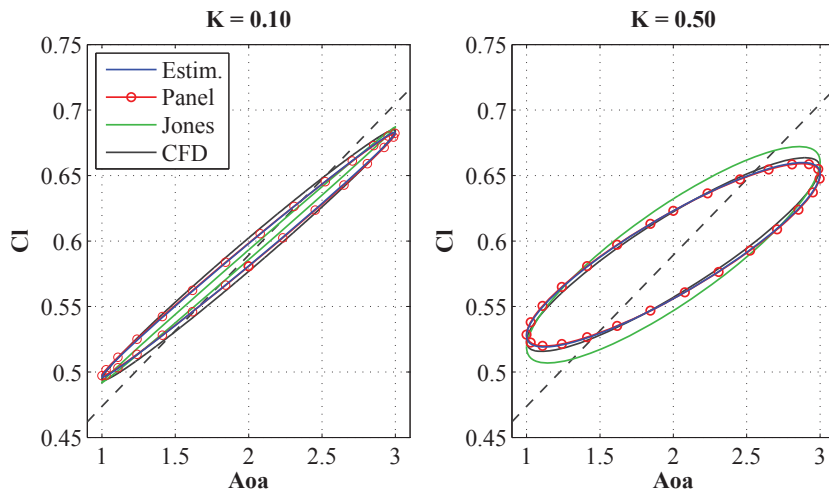
The turbulence seeds are kept the same among the three cases, and the effects on the loads are determined from the variation of the *equivalent fatigue loads* and *ultimate loads*. The equivalent fatigue loads are computed with a rain-flow-counting method²⁵ considering the production cases (DLC 1.1) specified in the IEC standard 61400-1.²⁶ Simulations are carried out for wind conditions corresponding to turbine class *Iib*, and a yaw misalignment of $\pm 8^\circ$ is included. The ultimate load is given by the maximum load among a reduced set of simulation cases from the same standard:²⁶ production with extreme turbulence model (DLC 1.3), extreme coherent gust (DLC 1.4), and extreme operating gust (DLC 2.3).



(a) NACA 64-418.



(b) DU 91-W2-250.



(c) RISOE A1-21.

Figure 6. Lift coefficient loops for airfoils undergoing harmonic pitching motion. Comparison between CFD results (black) and analytical model based on indicial response coefficients from: empirical estimation function (blue), panel code response (red line with circles), Jones's flat plate coefficients (green).

Table 2 reports the variation in the simulated fatigue and ultimate loads, expressed as percentage of the loads resulting from flat plate coefficients. The assumption of quasi steady attached flow dynamics (Q.St. rows) leads to higher loads; for instance, the equivalent fatigue loads for the blade root flapwise moment is increased by almost 6%, and similar variations are reported in the ultimate loads. By applying the lift response coefficient of the DU 91-W2-250 airfoil (DU 25 rows), the simulated wind turbine loads are lower; the difference is not as large as in the quasi-steady case, but, still, variations above one point percent are reported.

Although the quantitative figures might depend on the turbine and control used in these simulations, it can be concluded that model choices of attached flow aerodynamics have an effect on the estimation of the overall loading condition of the turbine.

		Blade Flapw.	Blade Edgew.	Blade Tors.	Tower FA	Tower SS	Tower Tors.	Shaft Tors.
Quasi-St.	(F)	5.93%	0.72%	28.79%	3.04%	6.02%	8.43%	10.24%
DU 250	(F)	-1.09%	-0.01%	-3.00%	-0.50%	-1.16%	-2.26%	-1.64%
Quasi-St.	(U)	3.72%	2.29%	25.26%	-1.94%	3.44%	6.07%	5.45%
DU 250	(U)	0.70%	-1.89%	-1.03%	-1.98%	1.72%	-2.19%	-1.02%

Table 2. Variations in the equivalent fatigue load (F) and ultimate load (U) for simulation run with: Quasi-Steady attached flow dynamics, DU 91-W2-250 lift response coefficients. Variations expressed as percentage of the loads computed with Jones’s flat plate coefficients.

VI. Conclusion

The unit lift response function for airfoil with finite thickness differs from the flat plate one; generally, the thicker the airfoil, the slower is the response, and the lower the starting value Φ_0 .

The investigation considered a dataset of airfoil shapes derived from the NACA 4-digits family with a modified thickness distribution. For each airfoil, the indicial lift response is obtained from panel code simulations, and then approximated by a two terms exponential function; the exponential function is similar to Jones’s flat plate one, and is defined by four response coefficients, eq. (6).

An empirical relation is found, where the four response coefficients are given as a function of the profile geometry. It is thus possible to estimate the indicial lift response of an airfoil from its geometric characteristics, namely the profile angle measured in three locations along the chord.

The empirical relation is tested with three airfoil profile shapes used on the MEXICO²⁰ reference rotor. The resulting estimated lift responses are very similar to the ones computed with the panel code; furthermore, the estimated indicial responses return unsteady lift loops that are closer to CFD results than the corresponding loops based on Jones’s flat plate response.

The effects of different indicial lift approximations on an overall load estimation have been quantified for the NREL 5-MW reference turbine²⁴ through aeroelastic simulations. The indicial response of finite thickness airfoils, which is slower than the flat plate one, results in slightly lower loads than obtained with Jones’s approximation; on the contrary, a quasi steady approximation leads to higher loads. The quantitative difference might vary with the turbine model, and the control strategy; in the investigated case the variation was in the order of $1 \sim 5\%$. Similarly, changes in the indicial lift approximations are also expected to return slightly different stability limits for the full turbine.

To conclude, a flat plate approximation is certainly preferable to a quasi steady one, but the outlined empirical relation could further improve the accuracy of the indicial response. Further testing might be required to generalize, and eventually tune, the empirical relation for other series of airfoil.

VII. Acknowledgments

It is gratefully acknowledged that this work is partly funded by the Danish project *Development of Adaptive Trailing Edge Flap (ATEF) System for Wind Turbines* by the Advanced Technology Foundation, Advanced Technology Projects 2007.

References

- ¹Beddoes, T. S., “Practical Computations of Unsteady Lift,” *Vertica*, Vol. 8, No. 1, 1984, pp. 55–71.
- ²Leishman, J. G. and Nguyen, K. Q., “State-Space Representation of Unsteady Airfoil Behavior,” *AIAA Journal*, Vol. 28, No. 5, 1990, pp. 836–844.

- ³Larsen, T. J., “How 2 HAWC2 the user’s manual,” Tech. Rep. R-1597(EN), Risø National Laboratory. Technical University of Denmark, 2009.
- ⁴Hansen, M. H., Gaunaa, M., and Madsen, H. A., “A Beddoes-Leishman type dynamic stall model in state-space and indicial formulations,” Tech. Rep. R-1354(EN), Risø National Laboratory, Roskilde (DK), 2004.
- ⁵Bossanyi, E., “GH Bladed Theory Manual,” Tech. rep., Garrad Hassan and Partners Ltd, 2003.
- ⁶Jonkman, J. M. and Buhl, M. L. J., “FAST User’s Guide - Updated August 2005,” Tech. Rep. NREL/TP-500-38230, National Renewable Energy Laboratory (NREL), 2005.
- ⁷Moriarty, P. J. and Hansen, A. C., “AeroDyn Theory Manual,” Tech. Rep. NREL/TP-500-36881, National Renewable Energy Laboratory (NREL), 2005.
- ⁸Theodorsen, T., “General theory of aerodynamic instability and mechanism of flutter,” Tech. Rep. 496, National Advisory Committee for Aeronautics (United States Advisory Committee for Aeronautics), 1935.
- ⁹Bisplinghoff, R. L., Ashley, H., and Halfman, R. L., *Aeroelasticity*, Dover Publications, Inc, 1996.
- ¹⁰Jones, R. T., “The unsteady lift of a wing of finite aspect ratio,” Tech. Rep. 681, National Advisory Committee for Aeronautics (United States Advisory Committee for Aeronautics), 1940.
- ¹¹Giesing, J. P., “Nonlinear two-dimensional unsteady potential flow with lift,” *Journal of Aircraft*, Vol. 5, 1968, pp. 135–143.
- ¹²Basu, B. C. and Hancock, G. J., “Unsteady Motion of a 2-Dimensional Aerofoil in Incompressible Inviscid Flow,” *Journal of Fluid Mechanics*, Vol. 87, No. JUL, 1978, pp. 159–178.
- ¹³Chow, C. Y. and Huang, M. K., “The Initial Lift and Drag of an Impulsively Started Airfoil of Finite Thickness,” *Journal of Fluid Mechanics*, Vol. 118, No. MAY, 1982, pp. 393–409.
- ¹⁴Gaunaa, M., *Unsteady Aerodynamic Forces on NACA 0015 Airfoil in Harmonic Translatory Motion*, Ph.D. thesis, Department of Mechanical Engineering, Technical University of Denmark, 2002.
- ¹⁵Buhl, T., Gaunaa, M., and Bak, C., “Potential load reduction using airfoils with variable trailing edge geometry,” *Transactions of the ASME. Journal of Solar Energy Engineering*, Vol. 127, No. 4, 2005, pp. 503–516.
- ¹⁶Bergami, L. and Gaunaa, M., “Stability investigation of an airfoil section with active flap control,” *Wind Energy*, Vol. 13, No. 2-3, 2010, pp. 151–166.
- ¹⁷Stack, J. and Doenhoff, A. E. V., “Tests of 16 related airfoils at high speed,” Tech. Rep. NACA-TR-492, National Advisory Committee for Aeronautics (United States Advisory Committee for Aeronautics), 1935.
- ¹⁸Hess, J., “Higher order numerical solution of the integral equation for the two-dimensional Neumann problem,” *Computer Methods in Applied Mechanics and Engineering*, Vol. 2, No. 1, 1973, pp. 1–15.
- ¹⁹Graham, J. M. R., “The Lift on an Aerofoil in Starting Flow,” *Journal of Fluid Mechanics*, Vol. 133, No. AUG, 1983, pp. 413–425.
- ²⁰Snel, H., Schepers, J. G., and Montgomerie, B., “The MEXICO project (Model Experiments in Controlled Conditions): The database and first results of data processing and interpretation,” *Journal of Physics: Conference Series*, Vol. 75, 2007, p. 012014.
- ²¹Michelsen, J. A., “Block structured Multigrid solution of 2D and 3D elliptic PDE’s,” Tech. Rep. AFM 94-06, Technical University of Denmark, 1994.
- ²²Michelsen, J. A., “Basis3D - A platform for Development of Multiblock PDE solvers,” Tech. Rep. AFM 92-05, Technical University of Denmark, 1992.
- ²³Sørensen, N. N., “General Purpose Flow Solver Applied to Flow over Hills,” Tech. Rep. Risø-R-827(EN), Risø National Laboratory, 1995.
- ²⁴Jonkman, J., Butterfield, S., Musial, W., and Scott, G., “Definition of a 5-MW Reference Wind Turbine for Offshore System Development,” Tech. Rep. NREL/TP-500-38060, National Renewable Energy Laboratory (NREL), Feb. 2009.
- ²⁵Hansen, M., *Aerodynamics of wind turbines : rotors, loads and structure*, James & James, London, 2000.
- ²⁶Commission, I. I. E., “IEC 61400-1: Wind Turbines Part 1: Design Requirements,” Tech. rep., International Electrotechnical Commission, 2005.